21st Australasian Fluid Mechanics Conference
Adelaide, Australia
10-13 December 2018

Flow Past a Diamond Cylinder at Moderate Reynolds Numbers

Hongyi Jiang[1], Liang Cheng[1,2], Hongwei An[1], Feifei Tong[1] and Fan Yang[1]

[1]Department of Civil, Environmental and Mining Engineering
The University of Western Australia, Crawley, Western Australia 6009, Australia

[2]State Key Laboratory of Coastal and Offshore Engineering
Dalian University of Technology, Dalian, Liaoning 116024, China

Abstract

Three-dimensional (3D) wake instabilities for flow past a diamond cylinder are investigated using direct numerical simulation. The neutral instability curve for mode A is mapped out, while that for mode B does not exist. Nevertheless, mode B flow structures are still captured in the fully developed 3D flows. The variations of the Strouhal number and drag coefficient with the Reynolds number are also presented.

Introduction

Steady incoming flow past a smooth and nominally two-dimensional (2D) bluff body is a classical problem in fluid mechanics. It is governed by a single dimensionless parameter, the Reynolds number Re (= UD/ν), which is defined based on the incoming flow velocity (U), the length scale of the cylinder perpendicular to the incoming flow (D), and the kinematic viscosity of the fluid (ν). For a circular cylinder the length scale is the diameter of the cylinder, while for a square cylinder aligned with sides perpendicular and parallel to the incoming flow (simply referred to as a square cylinder) the length scale is the side length of the cylinder. However, for a square cylinder aligned with all four sides 45 degrees to the incoming flow (referred to as a diamond cylinder), the length scale is $\sqrt{2}$ times the side length of the cylinder. To distinguish the length scales for a square and a diamond cylinder, the length scale for a diamond cylinder is denoted as h in this study.

The wake instabilities for flow past a circular and a square cylinder have been studied extensively in the literature by using physical experiments and direct numerical simulations (DNS) (e.g. Williamson, 1996; Jiang et al., 2016, 2018), where two three-dimensional (3D) wake flow structures have been discovered with increasing Re.

(i) The first 3D wake flow structure is a relatively large-scale mode A flow structure, with a spanwise wavelength of approximately $4D$ for a circular cylinder and approximately $5D$ for a square cylinder, and an out-of-phase sequence between the neighbouring streamwise vortices.

(ii) The second 3D wake flow structure is a finer-scale mode B flow structure, with a spanwise wavelength of approximately $0.8D$ for a circular cylinder and approximately $1.1D$ for a square cylinder, and an in-phase sequence between the neighbouring streamwise vortices.

In addition to the physical experiments and DNS, Floquet stability analysis has also been adopted to identify the 3D wake instability modes based on time-periodic 2D base flows. Both mode A and mode B and their neutral instability curves have been reported for the cases of a circular and a square cylinder (e.g. Barkley and Henderson, 1996; Park and Yang, 2016).

In contrast, for flow past a diamond cylinder only a mode A wake instability has been reported by Sheard et al. (2009) through Floquet stability analysis, while both mode A and mode B are observed through physical experiments (Tong et al., 2008) and DNS (Sheard et al., 2009). This study will complement previous studies on flow past a diamond cylinder by investigating the neutral instability curves of mode A and mode B and the 3D flow characteristics.

Numerical Model

Numerical Method

In the present study, the flow around a diamond cylinder is solved with DNS. The governing equations are the continuity and incompressible Navier-Stokes equations:

$$\frac{\partial u_i}{\partial x_i} = 0 \tag{1}$$

$$\frac{\partial u_i}{\partial t} + u_j \frac{\partial u_i}{\partial x_j} = -\frac{1}{\rho}\frac{\partial p}{\partial x_i} + \nu \frac{\partial^2 u_i}{\partial x_j \partial x_j} \tag{2}$$

where (x_1, x_2, x_3) = (x, y, z) are the Cartesian coordinates, u_i is the velocity component in the direction of x_i, t is the time, and p is the pressure. The numerical simulations are carried out with an open-source code OpenFOAM (www.openfoam.org). The finite volume method and the PISO (Pressure Implicit with Splitting of Operators) algorithm (Issa, 1986) are adopted for solving the equations. The convection, diffusion and time derivative terms are discretized, respectively, using a fourth-order cubic scheme, a second-order linear scheme, and a blended scheme consisting of the second-order Crank-Nicolson scheme and a first-order Euler implicit scheme, respectively. The same numerical formulation has been used in Jiang et al. (2016, 2018) for the simulations of flow past a circular and a square cylinder.

Computational Domain and Boundary Conditions

The 2D and 3D simulations adopt a rectangular and a hexahedral computational domain, respectively. As sketched in Fig. 1(a), the centre of the diamond cylinder is located at (x, y) = (0, 0). The computational domain size is $-40 \le x/h \le 40$ in the streamwise direction and $-40 \le y/h \le 40$ in the transverse direction. The blockage ratio in the transverse direction is 1.25%.

The boundary conditions are specified as follows. At the inlet boundary, a uniform flow velocity U is specified in the x-direction. At the outlet, the Neumann boundary condition (i.e., zero normal gradient) is applied for the velocity, and the pressure is specified as a reference value of zero. Symmetry boundary conditions are applied at the top and bottom boundaries, while periodic boundary conditions are employed at the two lateral boundaries perpendicular to the cylinder axis. For the lateral boundaries, Jiang et al. (2017a) showed that periodic boundary conditions are more suitable than symmetry boundary conditions in simulating fully developed

3D flows. A no-slip boundary condition is applied on the surface of the diamond cylinder.

(a)

(b)

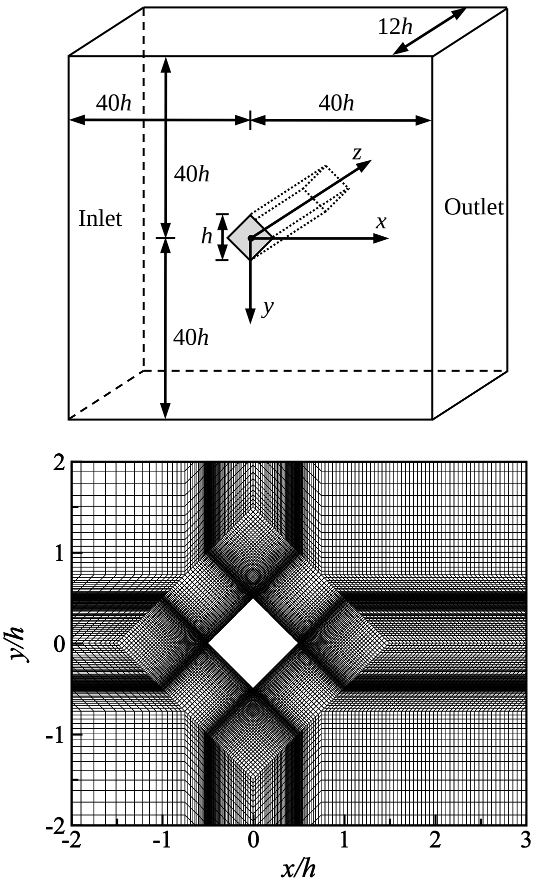

Fig. 1. (a) Schematic model of the computational domain (not to scale), and (b) Close-up view of the 2D mesh near the cylinder.

Computational Mesh

First, a 2D mesh is constructed in the *x*-*y* plane, namely the plane perpendicular to the cylinder axis. For the 2D mesh, the cylinder surface is discretized with 128 nodes. The height of the first layer of mesh next to the cylinder is 0.008*h*. The cell size at the four corners of the cylinder is 0.008$h\times$0.008*h*. To capture detailed wake flow structures, a relatively high mesh resolution is used in the wake region by specifying a streamwise mesh size at the wake centreline increasing linearly from 0.04*h* at x/h = 1.5 to 0.1*h* at x/h = 20. A total of 92,828 cells are used for the 2D mesh. A close-up view of the mesh near the cylinder is shown in Fig. 1(b).

At the beginning of the simulation, the internal flow follows an impulsive start. The time step size for each case is $\Delta tU/h$ = 0.00186, which is chosen based on a Courant–Friedrichs–Lewy (CFL) limit of less than 0.5.

The mesh convergence of the 2D mesh is checked at *Re* = 255 with two variations to the above-mentioned reference mesh:

(i) A mesh refined in the *x*-*y* plane with doubled numbers of cells in both *x*- and *y*-directions. Specifically, the number of cells around the cylinder surface is doubled from 128 to 256, while the height of the first layer of mesh next to the cylinder is halved from 0.008*h* to 0.004*h*. For this case, the time step size is also halved so as to satisfy the same CFL limit.

(ii) A mesh with a doubled computational domain size. The distance from the centre of the cylinder to each of the inlet, outlet, top and bottom boundaries increases from 40*h* to 80*h*.

Table 1 lists the hydrodynamic forces on the cylinder at *Re* = 255 calculated with different meshes. The drag coefficient (C_D) and the Strouhal number (*St*) are defined as:

$$C_D = F_D / (\rho U^2 h / 2) \quad (3)$$

$$St = f_L h / U \quad (4)$$

where F_D is the drag force on the cylinder, and f_L is the frequency of the fluctuating lift force. The time-averaged drag coefficient is denoted with an overbar. As shown in Table 1, the hydrodynamic forces calculated by the two variation cases are within 1% of those calculated with the reference mesh. Hence the reference mesh is used in the present study.

Case	*St*	$\overline{C_D}$
Reference	0.1967	1.8970
Refined mesh	+ 0.76%	+ 0.81%
Doubled domain size	– 0.49%	– 0.92%

Table 1. Mesh independence check of the hydrodynamic forces on the cylinder at *Re* = 255. The results other than the reference case are shown by the relative differences with respect to those of the reference case.

The 3D mesh is constructed by replicating the 2D mesh along the *z*-axis with a spanwise cell size of 0.1*h*. The secondary wake instability of flow past a diamond cylinder is a mode A wake instability (Sheard et al., 2009). As will be shown in the next section, the critical *Re* for the onset of mode A and the associated critical spanwise wavelength of mode A calculated in the present study are (Re_{cr}, $(\lambda/h)_{cr}$) = (120.7, 4.00). By using a spanwise cell size of 0.1*h*, 40 spanwise layers are used to capture one spanwise period of mode A structure. Such a spanwise mesh resolution is the same as those used in Jiang et al. (2016, 2018) for flow past a circular and a square cylinder. The spanwise domain length is 12*h*, namely three times the $(\lambda/h)_{cr}$ value, which is also the same as those used in Jiang et al. (2016, 2018) for flow past a circular and a square cylinder.

Numerical Results

Onset of Wake Instability

For flow past a circular or a square cylinder, the neutral instability curves of the 3D wake instability modes have been predicted by both Floquet stability analysis (e.g. Barkley and Henderson, 1996; Park and Yang, 2016) and DNS (Jiang et al., 2017b, 2018). Floquet stability analysis is performed based on a perfectly time-periodic 2D base flow (Barkley and Henderson, 1996). However, it is noted that the development of the secondary vortex street in the far wake of a bluff body would result in flow irregularity in time (Kumar and Mittal, 2012). For the 2D base flow in the wake of a circular or a square cylinder, the irregular secondary vortex street develops at more than 30*D* downstream of the cylinder for the wake transition regimes of $Re \lesssim 300$, while the near-wake flow is time-periodic, such that Floquet stability analysis can be performed by choosing a computational domain excluding the far-wake irregularities.

However, our 2D simulations show that for flow past a diamond cylinder the irregular secondary vortex street develops closer to the cylinder, for example at x/h = 14 for *Re* = 200 and at x/h = 7.5 for *Re* = 300. The irregular development of the secondary vortex street would also result in flow irregularity to a certain distance upstream of the onset of the secondary vortex street (which may be very close to the cylinder), and consequently Floquet stability analysis could not be performed precisely. For example, Floquet stability analysis was conducted by Sheard et al. (2009) for *Re* up to approximately 140, since Sheard et al. (2009) found that for *Re* ≳ 140 the 2D base flow became aperiodic. For *Re* ≲ 140, Sheard et al. (2009) identified a mode A wake instability at $(Re_{cr}, (\lambda/h)_{cr})$ = (116, 4.0).

To investigate the wake instabilities for *Re* ≳ 140, DNS has been adopted in the present study. The spanwise mesh resolution for one spanwise period of mode A is 20 layers of mesh. Fig. 2 shows the neutral instability curve of mode A for flow past a diamond cylinder calculated with DNS, determined through running simulations at small increments of *Re* around the neutral curve. The critical point at the left tip of the neutral curve is $(Re_{cr}, (\lambda/h)_{cr})$ = (120.7, 4.00).

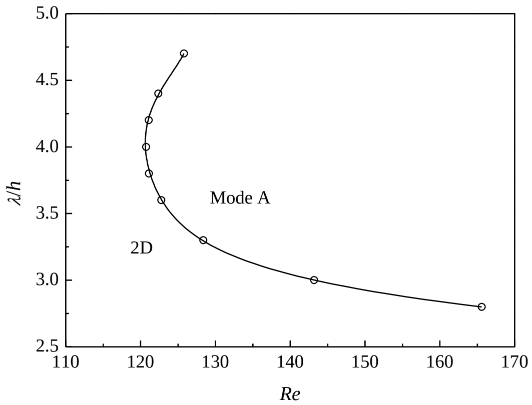

Fig. 2. Neutral instability curve of mode A for flow past a diamond cylinder.

A mesh convergence check of the Re_{cr} value is carried out with three variations of the mesh (with a fixed λ/h of 4.00):

(i) A mesh refined in the *x*-*y* plane with doubled numbers of cells in both *x*- and *y*-directions.

(ii) A mesh with a doubled computational domain size. In particular, the blockage ratio in the transverse direction reduces from 1.25% to 0.625%.

(iii) A mesh refined in the *z*-direction with doubled number of layers in the *z*-direction.

Table 2 shows the Re_{cr} values predicted with different meshes, which are all within 1% of that predicted with the reference mesh. It is also noticed that the Re_{cr} value reported in Sheard et al. (2009) is 3.89% smaller than the present result. Since a reduction in the blockage ratio from 1.25% (the reference case) to 0.0625% would result in a 0.75% increase in the Re_{cr} value (see Table 2), it is speculated that the 3.89% decrease in the Re_{cr} value by Sheard et al. (2009) is largely attributed to a relatively large blockage ratio of 3.54%.

Case	Re_{cr} (Relative difference)	Blockage ratio
Reference	120.7	1.25%
Refined in the *x*-*y* plane	120.6 (– 0.08%)	1.25%
Doubled domain size	121.6 (+ 0.75%)	0.625%
Refined in the *z*-direction	120.7 (+ 0%)	1.25%
Sheard et al. (2009)	116 (– 3.89%)	3.54%

Table 2. Mesh independence check of the Re_{cr} value.

In addition to the mode A wake instability, a mode B wake instability with a higher Re_{cr} value and a smaller $(\lambda/h)_{cr}$ value than those of mode A has been discovered for flow past a circular and a square cylinder (e.g. Barkley and Henderson, 1996; Park and Yang, 2016). The critical point for the onset of mode B from a 2D base flow is Re_{cr} = 259 for a circular cylinder (Barkley and Henderson, 1996) and Re_{cr} = 201.4 for a square cylinder (Jiang et al., 2018). However, for flow past a diamond cylinder, the mode B neutral instability curve is not discovered in the present study in the area below the lower branch of the neutral curve for mode A for *Re* ≤ 280.

Three-dimensional Flows

Fig. 3 shows the Strouhal number and time-averaged drag coefficient for flow past a diamond cylinder for *Re* = 60 – 280. The 2D hydrodynamic forces are calculated based on the time-histories of a complete vortex shedding cycle of the fully developed flow, since the fully developed 2D flows are time-periodic. However, the fully developed 3D flows are irregular in time. For each 3D case, the simulation is run for approximately 500 non-dimensional time units (defined as $t^* = Ut/D$) to obtain the fully developed flow. After that, approximately another 500 non-dimensional time units of the fully developed flow are used to calculate the fully developed hydrodynamic forces on the cylinder. For 3D flows, f_L in equation (4) is determined as the peak frequency derived from the fast Fourier transform (FFT) of the time-history of C_L.

As shown in Fig. 3, beyond the onset of the mode A instability at Re_{cr} = 120.7, the 3D results are slightly smaller than their 2D counterparts due to the flow three-dimensionality. Some typical 3D flow structures are shown in Fig. 4. At *Re* = 125, ordered mode A structures are observed at early stages of the simulation (Fig. 4a). However, the ordered mode A is an unstable state. With the evolution in time, vortex dislocations would appear in the entire wake region (Fig. 4b). This feature is similar to the case of flow past a circular and a square cylinder (Williamson, 1996; Jiang et al., 2018). For *Re* ≳ 200, mode B structures are observed in the wake (Fig. 4c,d), albeit the inexistence of the neutral instability curve of mode B for *Re* ≤ 280.

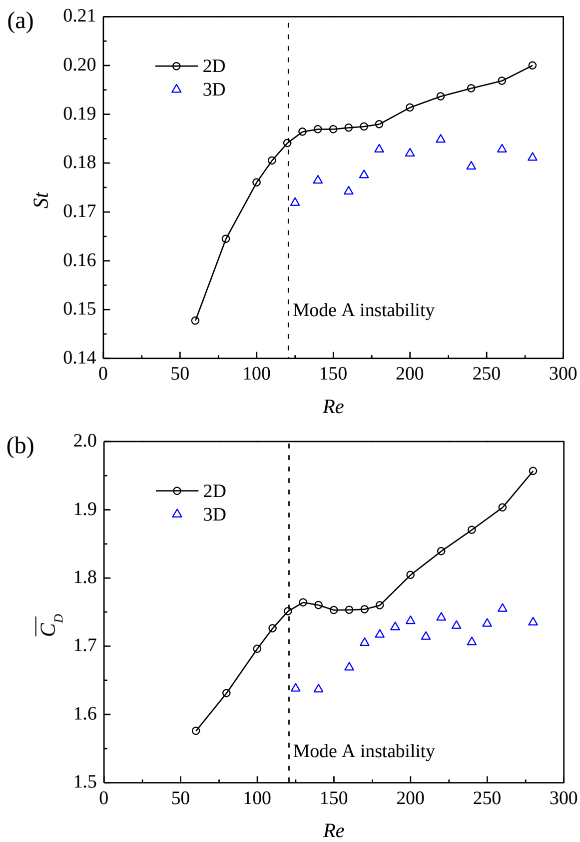

Fig. 3. Variations of the hydrodynamic forces with *Re* for flow past a diamond cylinder: (a) the Strouhal number, and (b) the time-averaged drag coefficient.

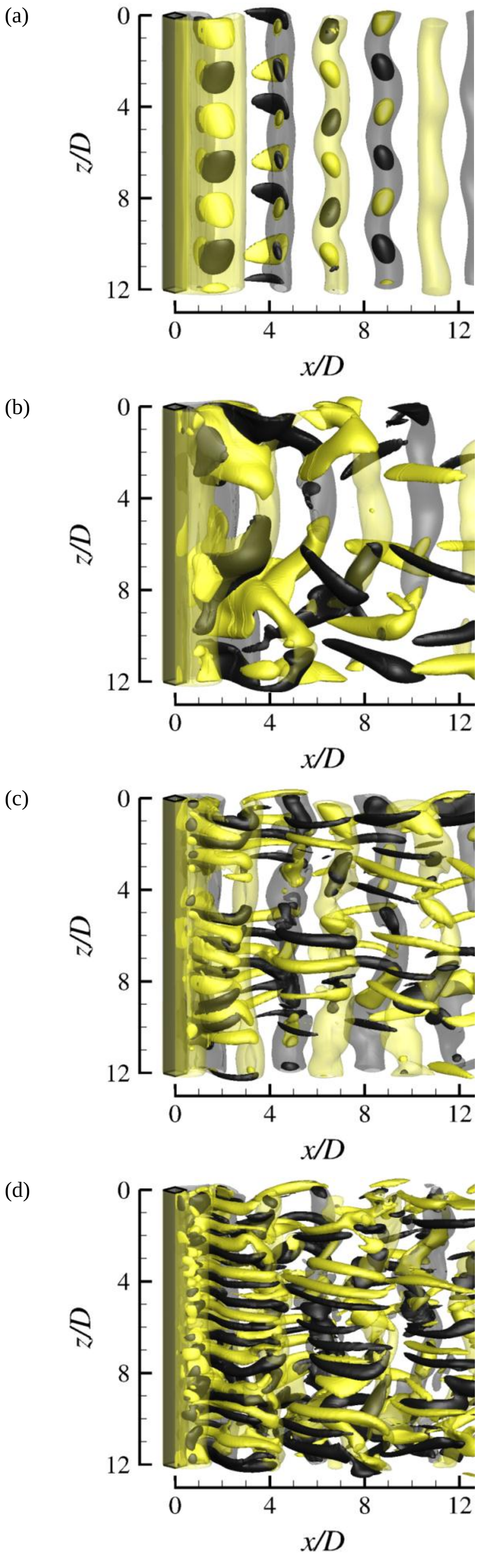

Fig. 4. Instantaneous vorticity fields in the near wake of a diamond cylinder for (a) Re = 125 and t^* = 400 (with ordered mode A structures), (b) Re = 125 and t^* = 900 (with disordered mode A having vortex dislocations), (c) Re = 200 and t^* = 1000 (with mode B structures), and (d) Re = 280 and t^* = 900 (with mode B structures). The translucent iso-surfaces represent spanwise vortices with $\omega_z = \pm 1.0$, while the opaque iso-surfaces represent streamwise vortices with $\omega_x = \pm 0.5$ for graphs (a) and (b) and $\omega_x = \pm 1.0$ for graphs (c) and (d). Dark grey and light yellow denote positive and negative vorticity values, respectively. The flow is from left to right past the cylinder on the left.

Conclusions

This paper presents a DNS study of the 3D wake instabilities and flow characteristics in the wake of a diamond cylinder. Due to the aperiodicity of the 2D base flow, the neutral instability curve of mode A is predicted with DNS rather than Floquet stability analysis. The critical point for the onset of mode A is $(Re_{cr}, (\lambda/h)_{cr})$ = (120.7, 4.00). It is also found that the mode B neutral instability curve does not exist for $Re \leq 280$. Nevertheless, mode B flow structures are still captured in the fully developed 3D flows for $Re \gtrsim 200$.

Acknowledgments

This work was supported by resources provided by the Pawsey Supercomputing Centre with funding from the Australian Government and the Government of Western Australia.

References

[1] Barkley, D., Henderson, R.D., 1996. Three-dimensional Floquet stability analysis of the wake of a circular cylinder. *Journal of Fluid Mechanics* 322, 215–241.

[2] Issa, R.I., 1986. Solution of implicitly discretized fluid flow equations by operator-splitting. *Journal of Computational Physics* 62, 40–65.

[3] Jiang, H., Cheng, L., Draper, S., An, H., Tong, F., 2016. Three-dimensional direct numerical simulation of wake transitions of a circular cylinder. *Journal of Fluid Mechanics* 801, 353–391.

[4] Jiang, H., Cheng, L., An, H., 2017a. On numerical aspects of simulating flow past a circular cylinder. *International Journal for Numerical Methods in Fluids*, 85, 113–132.

[5] Jiang, H., Cheng, L., Draper, S., An, H., 2017b. Prediction of the secondary wake instability of a circular cylinder with direct numerical simulation. *Computers & Fluids* 149, 172–180.

[6] Jiang, H., Cheng, L., An, H., 2018. Three-dimensional wake transition of a square cylinder. *Journal of Fluid Mechanics* 842, 102–127.

[7] Kumar, B., Mittal, S., 2012. On the origin of the secondary vortex street. *Journal of Fluid Mechanics* 711, 641–666.

[8] Park, D., Yang, K., 2016. Flow instabilities in the wake of a rounded square cylinder. *Journal of Fluid Mechanics* 793, 915–932.

[9] Sheard, G.J., Fitzgerald, M.J., Ryan, K., 2009. Cylinders with square cross-section: wake instabilities with incidence angle variation. *Journal of Fluid Mechanics* 630, 43–69.

[10] Tong, X.H., Luo, S.C., Khoo, B.C., 2008. Transition phenomena in the wake of an inclined square cylinder. *Journal of Fluids and Structures* 24, 994–1005.

[11] Williamson, C.H.K., 1996. Three-dimensional wake transition. *Journal of Fluid Mechanics* 328, 345–407.